Journal of Ceramic Processing Research. Vol. 14, No. 1, pp. 104~108 (2013)

J O U R N A L O F
Ceramic Processing Research

Growth behavior of low-dimensional nano ZnO on a biomorphic porous carbon (BPC) matrix by a hydrothermal synthesis method

Dong-yun Li[a], Peng-zhao Gao[b,*], Xiao-liang zhang[b], Shi-ting Huang[b], Ling Wang[b] and Han-ning Xiao[b]
[a]*College of Materials Science and Engineering, China Jiliang University, Hangzhou 310018, P.R.China*
[b]*College of Materials Science and Engineering, Hunan University, Changsha 410082, P.R.China*

In this paper, the growth behavior of low-dimensional nano ZnO on biomorphic porous carbon matrix (BPC matrix) by a hydrothermal synthesis method is studied. The Influence of the growth time, type of BPC matrix and its carbonization temperature on the growth behavior of nano ZnO are studied through XPS, XRD, TGA, SEM etc. The results show that hexagonal ZnO is obtained on a BPC matrix and the grain size is about 8 nm. Zero-dimensional nano-ZnO particles can grow on the inner walls of BPC matrix derived from hardwood, it is distributed evenly and combines well with the walls; while one-dimensional nano rods or two-dimensional nano sheets can grow on that of bamboo and two-dimensional nano sheets can grow on that of pine. The morphology, size and amount of nano-ZnO crystals are mainly controlled by growth time and matrix carbonization temperature, respectively. The growth mechanism of nano-ZnO crystal on a BPC matrix is also discussed.

Key words: Biomorphic porous carbon, Hydrothermal synthesis, Nano-crystal growth, XPS.

Introduction

ZnO gives an excellent performance in electronic, optic and photonic systems with a direct band gap of 3.37 eV and an exciton binding energy of 60 meV at room temperature [1-4]. The properties of the ZnO material are greatly affected by its preparation method, particle size, and morphology. Presently, one-dimensional (1D), 2D or 3D self-assembled ZnO such as nanobelts [5, 6], nanotubes [7, 8], aligned nanonails [9, 10], oriented ZnO nanorods [11, 12] have been prepared through different methods. Also they are usually deposited onto different substrates as Si, SiO_2, Al_2O_3 and C. Among these composites, ZnO/carbon composites are usually obtained by a solution combustion synthesis of ZnO and activated carbon mixtures [13-16], which can be used as an electrode for an electrochemical super capacitor [13, 14] and as a photo-catalytic catalyst [15, 16].

Compared with other "substrates", biomorphic porous carbon (BPC) matrix has the following advantages: it has a high specific surface area and an abundant amount of organic functional groups, which are propitious to improve the sensitivity of a sensor and catalytic activity when BPC works as a sensor and catalyst support [17]; The orderly, one-direction through-hole structure of BCP is very conducive to the transmission of material in which, a variety of pore size distributions for BPC provides different transmission channels [18]. However, little work has been done on the study of the growth behavior of low-dimensional nano-materials in BPC systemically.

A hydrothermal method is widely used to prepare many types of nano-materials. It has a low cost, environment-friendly characteristics, and can be done with simple equipment. The materials obtained exhibit high purity, crystal integrity,are mono-dispersed with shape and size control [19].

In this paper, the growth behavior of low-dimensional nano ZnO on a BPC matrices by a hydrothermal method is studied. The influence of the growth time, types of BPC matrix and its carbonization temperature on the growth behavior of low-dimensional ZnO are studied through XPS, XRD,TGA, SEM etc. Finally, the growth mechanism of ZnO on BPC matrix is discussed also.

Experiments

Raw materials

The biomorphic porous carbon derived from hardwood, pine and bamboo obtained retained their original characteristics of wood according to reference [20]. The BPC obtained was cut into small blocks 5 mm × 5 mm × 5 mm.

Cetyltrimethylammonium bromide (CTAB, $C_{19}H_{42}BrN$), Urea (CH_4N_2O), Zinc acetate ($Zn(CH_3COO)_2 \cdot 2H_2O$), Ethanol ($CH_3CH_2OH$) were used in there experiment. All chemical are obtained from Shanghai Chemical Corp, and were of AR grade. The water used in this experiment was deionized.

Preparation of low-dimensional nano-ZnO on BPC

0.11 g zinc acetate, 0.2 g urea and 0.05 g CTAB were

*Corresponding author:
Tel : +86-731-88822269
Fax: +86-731-88823554
E-mail: gaopengzhao7602@hnu.edu.cn

dissolved in 20 ml deionized water. The solution and blocks of BPC were added into a 25 ml Teflon lined stainless steel autoclave, filling 80% of the reactor capacity. The hydrothermal process was carried out at 150 °C for 5, 10 and 15 h. After that, the autoclave was cooled down naturally. The precipitate in the autoclave was collected and washed with deionized water and ethanol 3 times, all washing processes were operated in an ultrasonic washing machine. After that, the precipitate was dried in air at 80 °C for 6 h.

Characterization

The content of the organic groups in BPC was determined by XPS. XPS measurements were carried out with a Fisons Escalab 200R Ultra spectrometer, equipped with a monochromatic MgK_α X-ray source and a delay-line detector. Spectra were obtained using a magnesium anode (MgK_α = 1253.6 eV eV) operating at 150 W. The background pressure was 2×10^{-11} Mpa. The morphology of the nano ZnO-BPC material was characterized by scanning electron microscopy (SEM, JSM-6700F, Jeol). The pase of nano ZnO-BPC material was characterized by X-ray diffraction (XRD, D5000, Siemens), using nickel filtered Cu K_α radiation produced at 30 kV and 30 mA, with a scanning speed of 2 ° $minute^{-1}$. The crystal size of nano-ZnO was calculated by the Scheerer equation:

$$D = \frac{K\lambda}{B\cos\theta} \quad (1)$$

where λ is the wavelength, B the width of a half peak and K equals to 0.89.

The decomposition steps of the nano-material obtained was characterized using thermogravimetric analysis (TGA) and differential scanning calorimetry (DSC) in an Ar flow-rate of 50 ml · $minute^{-1}$ with a heating rate of 10 K · $minute^{-1}$ from room temperature to 800 °C. TGA and DSC were performed on a TGA-DSC (model Netzsch Thermische Analyzer STA 409C) thermal analyzer with alumina powder as the reference sample.

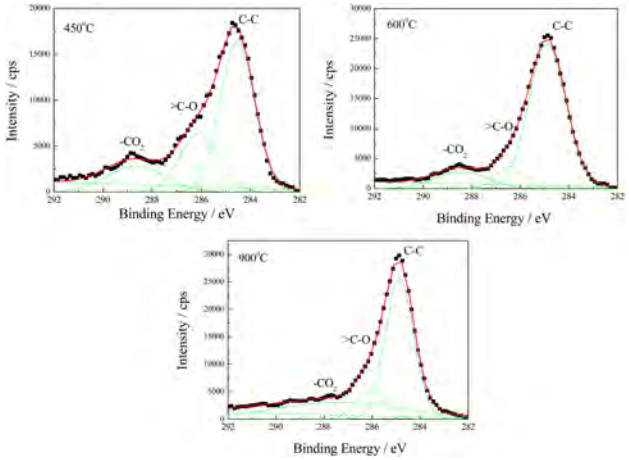

Fig. 1. C_{1s} XPS Spectra of pine wood carbonized at different temperatures.

Result and discussion

Influence of carbonization temperature on content of organic functional group of BPC

The C_{1s} XPS Spectra of BPC derived from pine carbonized at different temperatures are shown in Fig. 1, where $-CO_2$ stands for the oxo-organic functional group O - C = O, > CO for C-O and C-O-C, and C-C for the common C-C bond. The peak area in the XPS spectra stands for the content of the organic group in the BPC.

From Fig. 1, it is easy to see that there exists an abundant amount of oxo-organic groups in the BPC carbonized at 450 °C, as the carbonized temperature increases, the peak area of $-CO_2$ and > CO decreases, while that of C-C increases. Namely, as the temperature increases, the content of oxo-organic functional groups in the BPC decreases and the C-C group increases.

XRD analysis of nanoZnO- BPC materials

Fig. 2 shows the XRD pattern of nano ZnO-BPC (BPC matrix derived from pine, carbonized at 450 °C, with a growth time 15 h). Form the pattern, it is easy to see that the narrow and sharp peaks indicates a good crystalline state, which belongs to ZnO hexagonal crystals. The grain size is calculated to be about 8 nm according to Scheerer formula. The low and weak diffraction peaks of BPC are covered by the ZnO diffraction peaks [21].

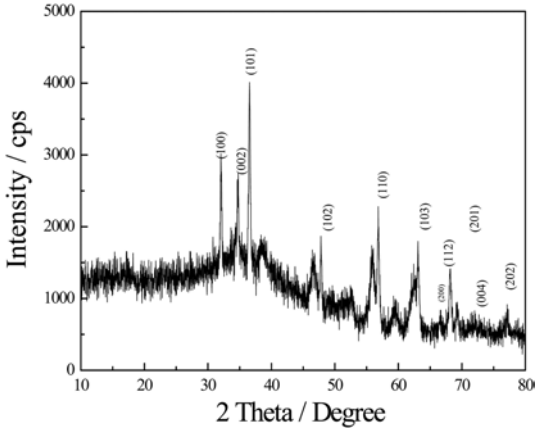

Fig. 2. XRD pattern of ZnO-BPC material.

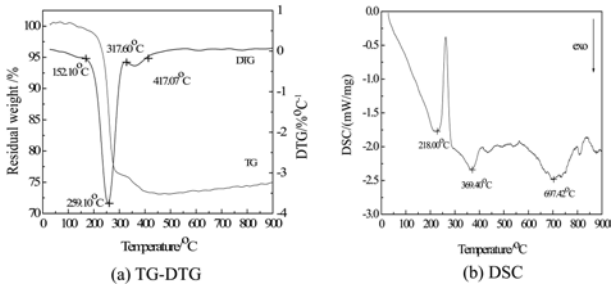

Fig. 3. TG-DTG and DSC curves of nano ZnO powder obtained in solution.

Thermal decomposition behavior of nano-ZnO powder

The TG-DTG and DSC curves of nano-ZnO powder obtained in solution are shown in Fig. 3. From the TG-DTG curves, it can be seen clearly that there is a small weight-loss before 152.10 °C, due to the evaporation of a small amount of water and organic solvent; the weight of the sample exhibits a sharp decline between 152.10 °C and 317.60 °C, the weight-loss peak is at 259.10 °C, suggesting the decomposition of residual urea in the sample; the weight appears with a slow decline between 317.60 °C and 417.07 °C corresponding to the decomposition of residual CTAB in the sample; the quality is almost unchanged after 417.07 °C. The weight loss is about 24.3% in all.

The DSC curve of the sample is shown in Fig. 3-b, exothermic peaks appear at 218.00 °C, 369.40 °C and 697.42 °C. Combined with the TG-DTG curve, the peaks at 218.00 °C and 369.40 °C correspond to the decomposition of residual urea and CTAB, respectively, while the peak at 697.42 °C is consistent with the phase transformation of crystal line ZnO [22].

Influence of the growth time on the microstructure of low-dimensional nano-ZnO

The microstructures of low-dimensional nano-ZnO on BPC (BPC derived from hardwood, carbonized at 450 °C) with different growth times are shown in Fig. 4. From Fig. 4-a, it is easy to see that the wall of the BPC is smooth and no particles can be observed. After 5 h growth, it can be seen that nucleation of ZnO occurs on the inner wall of the BPC, the nucleation of ZnO grows as the time increases. After 15 h growth, a large number of nano-ZnO particler can be seen grown on the inner wall of the BPC (Fig. 4-d), they are distributed evenly and exhibit a uniform size, which is about 60-100 nm. Thus, zero-dimensional nano-ZnO is obtained on the inner walls of the BPC, and the size of nano-particles can be controlled through changing the growth time.

Influence of the matrix type on the microstructure of low-dimensional nano-ZnO

The microstructure of ZnO obtained in solution and BPC matrices (BPC derived from hardwood, bamboo and pine, all carbonized at 450 °C, with a growth for 15 h) are shown in Fig. 5. From Fig. 5-a, it can be see clearly that the ZnO particles obtained in solution are severely agglomerated, the particle size exceeds 1 mm and the shape is sheet-line.

From Fig. 5-b, as mentioned above in Fig. 4-d, zero-dimensional nano ZnO can be seen grown on the inner wall of the BPC derived from hardwood. The diameter of the particle is about 60-100 nm, and they are combined tightly with wall surfaces. From Fig. 5-c, a mixture of ZnO nano-rods and nano-sheets can be seen grown on the inner wall of the BPC from bamboo. The length of the rods is about 100-200 nm and the

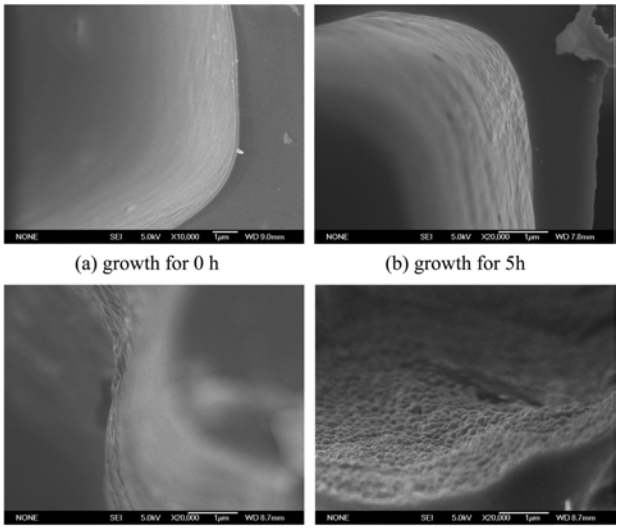

Fig. 4. SEM images of nano ZnO on BPC obtained with different growth times.

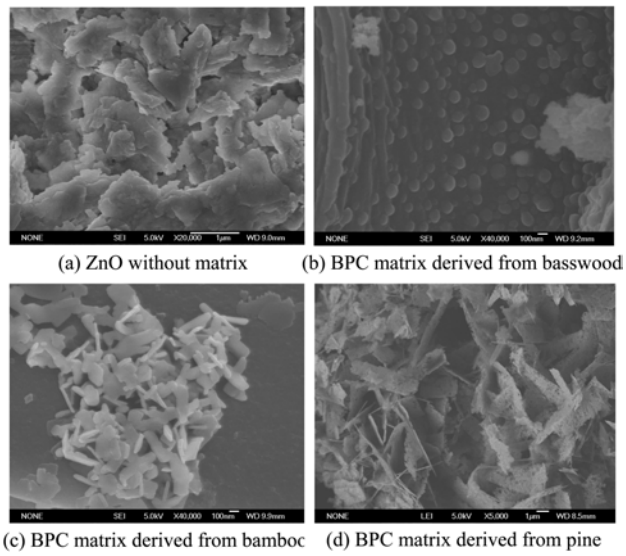

Fig. 5. SEM images of nano ZnO growth in solution and on BPC matrices derived from different types of wood.

diameter of them is about 50 nm, while the thickness of sheet is about 20-30 nm. From Fig. 5-d, it can be clearly seen that nano-ZnO thin sheet can be seen grown on the inner wall of the BPC from pine. The thickness of it is about 50 nm or so, the diameter varies.

Thus, the existence of a BPC can improve the mono-dispersed properties of nano-material during the hydrothermal process and also change the shape of it. Maybe there exists some “active points” in the BPC, which work as nucleation centers to avoid the agglomeration of ZnO. Furthermore, zero-dimensional nano ZnO particles can grow on the walls of the BPC derived from hardwood; one or two-dimemsional nano ZnO rod or sheet can grow on the BPC from bamboo and two-dimensional nano ZnO sheets can grow the BPC from pine. Different morphologies of low-

dimensional nano-ZnO are obtained on different BPC matrices. This phenomenon may result from the microstructure, specific area, pore size and organic group on the wall of a BPC derived from a different wood. This needs more research in the next step.

Influence of the BPC matrix carbonization temperature on the microstructure of low-dimensional nano-ZnO

The microstructures of low-dimensional nano-ZnO on BPC are shown in Fig. 6(BPC derived from pine, carbonized at 600 °C, 900 °C and grown for 15 h). Combined with Fig. 5-d, it is easy to see that the amount and the particle size of nano-ZnO on the inner walls of the BPC decrease with an increase of the BPC carbonization temperature. It is known that there exists an abundant amount of oxo-organic functional groups (such as O - C = O, C-O and C-O-C, etc) in a BPC when it is carbonized at 450 °C. The single pair electron of an O atom can coordinate with Zn^{2+} cation as an "active point" to increase the nucleation rate of ZnO crystals [23].

With an increase of the carbonization temperature, the content of oxo-organic functional groups on the walls of a BPC decreases. Namely, the amount of "active points" decreases, which also results in the amount of nano-ZnO decreasing. When the carbonization temperature of wood reachs 900 °C, most of the organic functional groups on the BCP decompose, as a result, it is difficult to grow ZnO on the inner wall of the BPC matrix(Fig. 6-b).

Discussion of the growth mechanism of nano-ZnO on a BPC matrix

According to the model of a growth unit, the growth process of a crystal is that acoordination ion in solution deposits on the nuclei interface as a growth unit, the coordination number of it is the same as that of an ion or atom in the crystal. It is known that zinc and oxygen are presented as $[ZnO_4]$ and $[OZn_4]$ with tetrahedral coordination of Zn and O atoms existing in the center of the tetrahedral structure in ZnO crystal [23].

So the Zn^{2+} and OH^- ion in solution forms ion complexes as $[Zn(OH)_4]^{2-}$ first, then the units grows through a dehydration reaction or coordination reaction between two "monomers", triple "monomers", four "monomers"·····, which combine into the crystal with a certain structure. The remaining OH^- ions present in the surface of these strucutres and is exposes every vertex of the coordination polyhedra, edge or face, then it continues to combine the growth units to form ZnO crystals until consumed.

The reaction steps are as following [24] :

$$Zn^{2+} + 4OH^- = [Zn(OH)_4]^{2-} \quad (2)$$

$$[Zn(OH)_4]^{2-} + [Zn(OH)_4]^{2-} = [Zn_2O(OH)_6]^{4-} + H_2O \quad (3)$$

$$[Zn_2O(OH)_6]^{4-} + [Zn(OH)_4]^{2-} = [Zn_3O_2(OH)_7]^{5-} + H_2O + OH^- \quad (4)$$

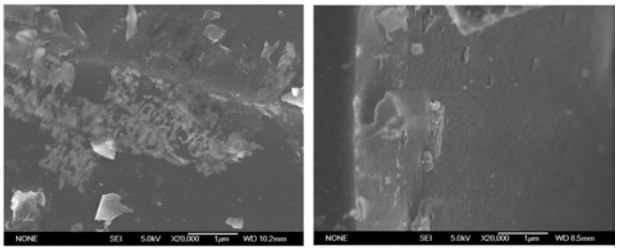

(a) BPC matrix carbonized at 600°C (b) BPC matrix carbonized at 900°C

Fig. 6. SEM images of nano ZnO growth on a BPC matrix (pine carbonized at 600 and 900 °C, respectively).

From the above discussion, we know that the dangling bonds on each surface of a grain is OH^-. So the growth rate of each face depends on the number of dangling OH^- bonds exposed to the solution. Therefore, according to the law of the growth habit and the coordination polyhedra, each face has a different number of angles, edges or faces exposed to the solution. So the growth rate in each direction is different. The crystal growth rate of ZnO in different directions is $V_{[00\bar{1}]} > V_{[001]} > V_{[\bar{1}01]} > V_{[\bar{1}00]}$ [24]. As the growth time increase, the grains grow up to become slender nano rods as in Ref [25].

In this study, urea in solution can decompose to produce OH^-, then the OH^- can react with Zn^{2+} to produce $[Zn(OH)_4]^{2-}$. CTAB can coordinate with OH^- which is exposed to solution and the BPC can work as the "active points".

It is known that there are an abundance of oxo-organic functional groups (such as O - C = O, C-O and C-O-C, etc) when a BPC matrix is carbonized at 450 °C, a single electron pair of an O atom in an oxo-organic functional group could react with a Zn^{2+} cation as an "active point" to increase the nucleation rate of ZnO crystals as seen in Fig. 5-b,c and d. Also the stable "active point" in BPC can help prevent agglomeration of nano-crystals as seen in Fig. 5-a and b. With an increase of the carbonization temperature, the amount of oxo-organic functional groups on BPC decreases, resulting in a decrease in the amount of nano-ZnO on inner wall of BPC also.

The crystal nucleation and growth processes of nano-ZnO on BPC matrix are as follows:

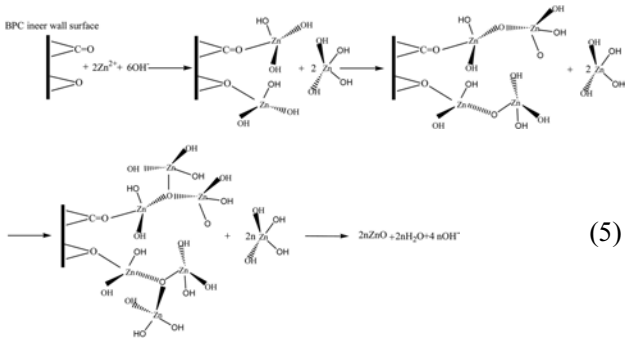

(5)

There are two functions of "CTAB" on nano-ZnO crystal growth during the hydrothermal process :

First, the combination of CTAB and $[Zn(OH)_4]^{2-}$ can decrease the crystal growth rate to obtain nano-scale material since the large volume of CTAB can hinder other groups or $[Zn(OH)_4]^{2-}$ to approach and react with the ZnO nucleus, as seen in the following equation:

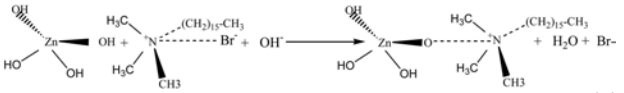

(6)

Second, there exists the largest amount of dangling OH^- bonds in the $[00\bar{1}]$ direction in a ZnO crystal. The combination of CTAB and $[Zn(OH)_4]^{2-}$ can decrease the growth rate very clearly in this direction for the "space restrain" of the large group, while that of other direction will be hindered less or not at all. So in this experiment, the morphologies of the nano-ZnO obtained are particles, rods and sheets.

Conclusions

1. As the carbonization temperature of a BPC increases, the content of oxo-organic functional groups in BPC decreases and that of C-C group increases.
2. Hexagonal ZnO is obtained under reaction conditions and the grain size is about 8 nm;
3. Zero-dimensional nano ZnO particles can grow on the inner walls of a BPC derived from hardwood, and one-dimemsional nano ZnO rods can grow on that from bamboo and two-dimensional nano ZnO sheets can grow on that from pine; The morphology, size and amount of nano-ZnO on a BPC substrate can be controlled through a change in the growth time and carbonization temperature of the BPC;
4. The nano ZnO growth mechanism is that an O atom of an oxo-organic functional group on the inner wall of BPC works as an "active point" to bond with Zn^{2+} to improve the nucleation rate of ZnO; CTAB can coordinate with OH^- to inhabit the growth rate in the $[00\bar{1}]$ of ZnO, which leads to the morphologies of nano-ZnO exhibiting particles, sheets and rods. The stable "active point" in BPC can help to prevent agglomeration of nano crystals.

Acknowledgement

This work was supported by the Natural Science Foundation of Hunan Province, China (Grant No. 12JJ4054) and the Science and Technology planning Project of Hunan Province, China (2012WK3023).

References

1. T.J. Sun, J.S. Qiu, C.H. Liang, J. Phys. Chem. C. 112 (2008) 715-721.
2. B.Q. Cao, X.M. Teng, S.H. Heo, Y. Li, S.O. Cho, G.H. Li, W.P. Cai, J. Phys. Chem. C. 111 (2007) 2470-2476.
3. L. Zhang, J. Li, X.W. Zhang, D.B. Yu, H.P. LinKhizar-ul-Haq, X.Y. Jiang, Z.L. Zhang, Curr. Appl Phy. 10 (2010) 1306-1308.
4. D.S. Kang, H.S. Lee, S.K. Han, V. Srivastava, E.S. Babu, S. Hong, M.J. Kim, J.H. Song, J.H. Song, H. Kim, D. Kim, J. Alloys Compd. 509 (2011) 5137-5141.
5. J. Zhang, W.Y. Yu, L.D. Zhang, Phys. Lett. A . 299 (2002) 276-281.
6. Y.X. Chen, X.Q. Zhao, J.H. Chen, Mater. Lett. 62 (2008) 2369-2371.
7. M.G. Fu, G.P. Du, X. Fu, B.F. Liu, Y.Q. Wan, L. Guo, Mater. Res. Bull. 43 (4) (2008) 912-918.
8. J.S. Jeong, J.Y. Lee, J.H. Cho, H.J. Suh, C.J. Lee, Chem. Mater. 17 (2005) 2752-2756.
9. J.Y. Lao, J.Y. Huang, D.Z. Wang, Z.F. Ren, Nanoletter. 3 (2003) 235-238.
10. X.H. Zhang, Y. Zhang, J. Xu, Z. Wang, X.H. Chen, D.P. Yu, Appl. Phys. Lett. 87 (2005) 123111 1-3.
11. C. Li, G.J. Fang, N.S. Liu, J. Li, L. Liao, F.H. Su, G.H. Li, X.G. Wu, X.Z. Zhao, J. Phys. Chem. C 111 (2007) 12566-12571.
12. C.H. Chao, C.H. Chan, J.J. Huang , L.S. Chang, H.C. Shih, Curr. Appl. Phy. 11 (2011) S136-S139.
13. .M. Jayalakshmi, M. Palaniappa, K. Balasubramanian, Int. J. Electrochem. Sci. 3 (2008) 96-103.
14. D. Kalpana, K.S. Omkumar, S. Suresh Kumar, N.G. Renganathan, Electrochim. Acta. 52 (2006) 1309-1315.
15. N. Sobana, M. Swaminathan, Sol. Energy Mater. Sol. Cells. 91 (2007) 727-734.
16. K. Byrappa, A.K. Subramani, S. Ananda, K.M. Lokanatharai, M.H. Suntha, B. Basavalingu, K. Soga, J. Mater. Sci. 41 (2006) 1355-1362.
17. M, Li, Y.L. Liu, P. Z. Gao, W. Chen , Z. X. Fu, Rare met. mater. eng. 38 [4] (2009) 734-737.
18. P.Z. Gao, Y.M. Bai, S. Lin, W.M. Guo, H.N. Xiao. Ceram. Intern. 34 (2008) 1975-1981.
19. Y. Zeng, T. Zhang, L. Qiao. Mater. Let. 63 (2009) 843-846.
20. P.Z. Gao, M.J. Wu, B.J. Li, Y.L. Liu. Mater. Re. Bull. 44 (2009) 644-648.
21. Z.J. Li, Z. F. Hu, F, J. Liu, J. Sun, H.Q. Huang, X. Zhang, Y.S. Wang, Mater. Let. 65 (2011) 809-811.
22. F. Davar, M.S. Niasari. J. Alloys Compd. 509 (2011) 2487-2492.
23. J. Xie, H. Wang, M. Duan, L.H. Zhang, Appl. Surf. Sci. 257 (2011) 6358-6363
24. U.N. Maiti, S. Nandy, S. Karan, Appl. Surf. Sci. 254 (2008) 7266-7271.
25. S.L. Bai, L.Y. Chen, D.Q. Li, W.S. Yang, P.C. Yang, Z.Y. Liu, A.F. Chen, C.L. Chung. Sen. Actu B 146 (2010) 129-137.